INDIAN JOURNAL OF SCIENCE AND TECHNOLOGY

ORIGINAL ARTICLE

Haar Wavelet Based Numerical Method to Solve Nonlinear Differential Equations Arising in Turbulent Boundary Layer Fluid Flow

S. C. Shiralashetti[1]*, S. S. Joshi[1], S. I. Hanaji[2]*

1 Department of Mathematics, Karnatak University, Dharwad-580003, Karnataka, India
2 KLE Technological University, Dr. M. S. Sheshgiri College of Engineering and Technology, Udyambag, Belagavi-590008, Karnataka, India

OPEN ACCESS

Received: 17/12/2024
Accepted: 06/02/2025
Published: 23/04/2025

Citation: Shiralashetti SC, Joshi SS, Hanaji SI (2025) Haar Wavelet Based Numerical Method to Solve Nonlinear Differential Equations Arising in Turbulent Boundary Layer Fluid Flow. Indian Journal of Science and Technology 18(13): 1046-1058. https://doi.org/10.17485/IJST/v18i13.4048

* **Corresponding authors**.

scshiralashetti@kud.ac.in

Funding: None

Competing Interests: None

Published By Indian Society for Education and Environment (iSee)

ISSN
Print: 0974-6846
Electronic: 0974-5645

Abstract

Objectives: To establish the Haar wavelet approach for solving the generalized Blasius equation, specifically in the context of turbulent flow at high Reynolds numbers. **Methods:** By employing an appropriate similarity transformation, the governing nonlinear partial differential equations describing turbulent boundary layers are reduced to ordinary differential equation. The Haar wavelet integration operational matrix method is developed to solve these governing equations for turbulent boundary layer fluid flow. **Findings:** The applicability of the proposed approach is illustrated by solving a nonlinear ordinary differential equation with an exact solution. Our results indicate that this method produces favourable results compared to the Range-Kutta Fehlberg 4^{th}-5^{th} Method. Furthermore, the effects of several parameters, such as acceleration and velocity, are examined at high Reynolds numbers. The findings are presented using tables and graphs. **Novelty:** Most previous research addressing the Blasius equation has focused on laminar flow. This article uniquely concentrates on solving the Blasius equation for turbulent flow. To our knowledge, wavelet numerical methods have not been applied to tackle these challenges in existing literature. The Haar wavelet method is particularly noted for its efficiency and accuracy, and we leverage this method to solve the turbulent boundary layer equations effectively.

Keywords: Haar wavelet method; Turbulent boundary layer; Blasius equation; Reynolds numbers; Nonlinear ODE

1 Introduction

A rise in Reynolds number in fluid dynamics usually results in a transition from laminar to turbulent flow characteristics [(1)]. In this context study of velocity and acceleration for high Reynolds numbers is crucial. Many problems associated with turbulent boundary layers have significant applications in science and engineering, including aircraft design, pipelines and fluid transport, heat exchangers and turbomachinery designs etc. The first to study the fundamentals of boundary layer theory was Ludwig

Prandtl in 1904. Combining two different disciplines hydraulics and hydrodynamics. Which provides solutions to Navier-Stokes equations at high Reynolds numbers. Later, Blasius [2] published an equation that describes the velocity profile within a laminar boundary layer over a continuous flat plate, laying the groundwork for the study of fluid behaviour near solid surface. Khanfer et al. [3] provided an approximate solution to the Blasius equation with temperature-dependent viscosity. Extensive research has been carried out on the study of turbulent boundary layers. The numerical simulation of a turbulent boundary layer over a flat plate is studied by Huang et al. [4] Laguarda et al. [5] investigated the effect of Reynolds number on turbulent boundary layers. Camillo et al. [6] examined the hypersonic turbulent boundary layer using both computational and experimental methods while taking massive eddies into account. The impact of an elastic panel on a turbulent boundary layer is analysed by Gao et al. [7] Additional related studies on turbulent boundary layers can be found in references [8], [9], [10].

Previously, the similarity solution, finite difference method (FDM), finite volume method (FVM), finite element method (FEM), and spectral approaches were the most widely used numerical techniques for solving such problems. FDM and FVM are approximations of the equation itself. Despite having global support, spectral bases are indefinitely differentiable. Conversely, base functions employed in finite element or finite difference methods have weak continuity qualities but small compact support. In conclusion, FDM, FVM, and FEM have strong spatial localization but low accuracy. Whereas spectral approaches have good accuracy but poor spatial localization. However, wavelets get around the limitation by offering precise and compact support both locally and globally.

In mathematical and application-oriented research areas wavelet analysis plays a vital role. Obtaining solutions for highly nonlinear ordinary and partial differential equations is a complex task, but wavelet methods simplify this process. Wavelets are commonly used in numerical analysis, image processing, signal analysis, and data compression. A very useful and efficient way to solve differential equations is the Haar wavelet approach, which allows for easy computation and improved convergence as the level of resolution increases. Construction of an operational matrix for Haar wavelets for the solution of fractional equation is given by Sunthrayuth et al. [11] Verma et al. [12] provided a Haar wavelet solution for a nonlinear system of singular differential equations using the collocation method. The numerical solution for the integro-differential equation by the Haar wavelet collocation method is discussed by Mohammad et al. [13] Preetham et al. [14] analysed magnetohydrodynamic (MHD) boundary layer nanofluid flow through the Haar wavelet numerical method. The algebraic multigrid approach utilizing Haar wavelets was applied by Shiralashetti et al. [15] to address the porous journal-bearing lubrication problem. Furthermore, Shiralashetti et al. [16] studied the Haar wavelet collocation method and provided solutions to Stochastic ordinary differential equations. Numerous authors have explored solutions to the Blasius equation for laminar flow [17], [18], [19], yet the application of wavelets to turbulent flow remains largely unexamined. Haar wavelet offers better accuracy and a simple approach for tackling complex problems. In this paper, we establish the formulation of the Haar wavelet integration operational matrix method (HWIOMM) to solve the generalized Blasius equation for turbulent flow obtained from governing equations of the two-dimensional turbulent boundary layer.

The structure of the paper is outlined as follows: Section 2 presents the methodology, detailing the Haar wavelet and its fundamental properties. This section also discusses the numerical computation of the Haar wavelet and its implementation in fluid dynamics problems. Section 3 reviews the results and discussions of the work, while Sections 4 and 5 are dedicated to the conclusion and references, respectively.

2 Methodology

2.1 Explanation of Wavelet and Haar Wavelet

Wavelets and wavelet-based analysis are utilized across a wide range of scientific and engineering fields. Wavelets consist of a set of functions derived from a single function known as the mother wavelet, which is modified through translation and dilation. Mathematically, a family of continuous wavelets is expressed as,

$$\psi_{(\alpha,\beta)}(x) = |\alpha|^{\frac{-1}{2}} \psi\left(\frac{x-\beta}{\alpha}\right), \alpha,\beta \in R, \alpha \neq 0. \tag{1}$$

Where α is dilation and β is translation parameters. To discretize the values, parameters are limited as, $\alpha = \alpha_0^{-j}, \beta = m\beta_0\alpha_0^{-j}, \alpha_0 > 1, \beta_0 > 0$ and $j,k \in Z$. The family of discrete wavelets are written as,

$$\psi_{j,k}(x) = |\alpha_0|^{\frac{j}{2}} \psi\left(\alpha_0^j x - k\beta_0\right), \tag{2}$$

where $\psi_{j,k}(x)$ represents wavelet bases for $L^2(R)$. Specifically, the function $\psi_{j,k}(x)$ represents an orthonormal basis when $\alpha_0 = 2$ and $\beta_0 = 1$. The Haar wavelet is the most basic orthonormal wavelet supporting compactly in $[0,1]$. The fundamental of the Haar wavelet family is the Haar scaling function and the Haar wavelet function defined as,

$$h_0(\eta) = \begin{cases} 1 & for\ \eta \in [0,1), \\ 0 & otherwise. \end{cases}$$
$$h_1(\eta) = \begin{cases} 1 & for\ \eta \in \left[0, \frac{1}{2}\right), \\ -1 & for\ \eta \in \left[\frac{1}{2}, 1\right), \\ 0 & otherwise. \end{cases} \tag{3}$$

Likewise, all other levels of wavelets can be generated from the translation and dilation of $h_1(\eta)$. In general, for $\eta \in [A,B]$ interval is divided into n subintervals, each of width $\Delta\eta = \frac{(B-A)}{n}$. The Haar wavelet is defined as,

$$h_k(\eta) = \begin{cases} 1 & for\ \eta \in [\zeta_1(k), \zeta_2(k)), \\ -1 & for\ \eta \in [\zeta_2(k), \zeta_3(k)), \\ 0 & otherwise. \end{cases} \tag{4}$$

Where,

$$\begin{aligned} \zeta_1(k) &= A + \left(\frac{p}{q}\right)(B-A) = A + \left(\frac{p}{q}\right) n\Delta\eta, \\ \zeta_2(k) &= A + \left(\frac{p+0.5}{q}\right)(B-A) = A + \left(\frac{p+0.5}{q}\right) n\Delta\eta, \\ \zeta_3(k) &= A + \left(\frac{p+1}{q}\right)(B-A) = A + \left(\frac{p+1}{q}\right) n\Delta\eta. \end{aligned} \tag{5}$$

Here, $q = 2^r, r = 0,1,...,J$ represents the dilation parameter, J is the maximum degree of resolution and $p = 0,1,2,...,q-1$ represents the translation parameter and the index k is given by $k = p+q+1$. Index k holds the minimum value of 2 for $q = 1$, p $= 0$ and maximum value of $N = 2M = 2^{J+1}$.

2.2 Haar Wavelet Function Approximation

Any function $f(\eta) \in L^2$ representing the Haar series can be expressed as,

$$f(\eta) = a_0 h_0(\eta) + a_1 h_1(\eta) + a_2 h_2(\eta) + ... = \sum_{k=0}^{\infty} a_k h_k(\eta).$$

Where $a_k, k = 0,1,2,...$, Haar coefficients and are given by, $a_k = \int_0^1 f(\eta) h_k(\eta) d\eta$.
If $f(\eta)$ is approximated in each sub-interval, then truncated infinite series will be,

$$f(\eta) \approx \sum_{k=0}^{q-1} a_k h_k(\eta) = A_k^T H_q(\eta). \tag{6}$$

Where $q = 2^r$. The Haar wavelet coefficient vector A_k and Haar wavelet function vector $H_q(\eta)$ are defined as, $A_k = [a_0, a_1, a_2, ..., a_{q-1}]^T, H_k(\eta) = [h_0, h_1, h_2, ..., h_{q-1}]^T$
Considering collocation points as following $\eta_r = \frac{2r-1}{2N}, r = 1,2,...,N$.
The Haar wavelet matrix $H_q(\eta)$ of order N for N collocation points is written as,

$$H_q(\eta) = \begin{bmatrix} h_0 \\ h_1 \\ h_2 \\ \vdots \\ h_{q-1} \end{bmatrix} = \begin{bmatrix} h_{0,0} h_{0,1} ... h_{0,q-1} \\ h_{1,0} h_{1,1} ... h_{1,q-1} \\ h_{2,0} h_{2,1} ... h_{2,q-1} \\ \vdots\vdots\vdots \\ h_{q-1,0} h_{q-1,1} ... h_{q-1,q-1} \end{bmatrix} \tag{7}$$

2.3 Haar Wavelet Integration Operational Matrix Method

Integration of the Haar wavelet vector $H_q(\eta)$ is approximated as,

$$\int_0^{\eta} H_q(\eta)d\eta \cong PH_q(\eta). \tag{8}$$

Where P forms operational matrix for Haar wavelet integration.
General order Haar wavelet integration operational matrix P_ν is expressed as,

$$P_\nu H_q(\eta) = [Ph_0(\eta), Ph_1(\eta), ..., Ph_{q-1}(\eta)]^T. \tag{9}$$

Where,

$$Ph_k(\eta) = \begin{cases} \frac{1}{\nu!}(\eta-\zeta_1(k))^\nu & \text{for } \eta \in [\zeta_1(k), \zeta_2(k)), \\ \frac{1}{\nu!}\{(\eta-\zeta_1(k))^\nu - 2(\eta-\zeta_2(k))^\nu\} & \text{for } \eta \in [\zeta_2(k), \zeta_3(k)), \\ \frac{1}{\nu!}\{(\eta-\zeta_1(k))^\nu - 2(\eta-\zeta_2(k))^\nu + (\eta-\zeta_3(k))^\nu\} & \text{for } \eta \in [\zeta_3(k), B), \\ 0 & otherwise. \end{cases} \tag{10}$$

Where,

$$\begin{aligned} \zeta_1(k) &= A + \left(\frac{p}{q}\right)(B-A) = A + \left(\frac{p}{q}\right) n\Delta\eta, \\ \zeta_2(k) &= A + \left(\frac{p+0.5}{q}\right)(B-A) = A + \frac{p+0.5}{q} n\Delta\eta, \\ \zeta_3(k) &= A + \left(\frac{p+1}{q}\right)(B-A) = A + \frac{p+1}{q} n\Delta\eta. \end{aligned} \tag{11}$$

For instance, if $J = 1 \Rightarrow N = 4, \eta \in [0,1)$,

$$P_1 H_4(\eta) = \frac{1}{8}\begin{bmatrix} 1 & 3 & 5 & 7 \\ 1 & 3 & 3 & 1 \\ 1 & 1 & 0 & 0 \\ 0 & 0 & 1 & 1 \end{bmatrix},$$

$$P_2 H_4(\eta) = \frac{1}{128}\begin{bmatrix} 1 & 9 & 25 & 49 \\ 1 & 9 & 23 & 31 \\ 1 & 7 & 1 & 1 \\ 0 & 0 & 1 & 7 \end{bmatrix},$$

If $J = 3 \Rightarrow N = 16, \eta \in [0,1)$,

$$P_1 H_{16}(\eta) = \frac{1}{32}\begin{pmatrix} 1 & 3 & 5 & 7 & 9 & 11 & 13 & 15 & 17 & 19 & 21 & 23 & 25 & 27 & 29 & 31 \\ 1 & 3 & 5 & 7 & 9 & 11 & 13 & 15 & 15 & 13 & 11 & 9 & 7 & 5 & 3 & 1 \\ 1 & 3 & 5 & 7 & 7 & 5 & 3 & 1 & 0 & 0 & 0 & 0 & 0 & 0 & 0 & 0 \\ 0 & 0 & 0 & 0 & 0 & 0 & 0 & 0 & 1 & 3 & 5 & 7 & 7 & 5 & 3 & 1 \\ 1 & 3 & 3 & 1 & 0 & 0 & 0 & 0 & 0 & 0 & 0 & 0 & 0 & 0 & 0 & 0 \\ 0 & 0 & 0 & 0 & 1 & 3 & 3 & 1 & 0 & 0 & 0 & 0 & 0 & 0 & 0 & 0 \\ 0 & 0 & 0 & 0 & 0 & 0 & 0 & 0 & 1 & 3 & 3 & 1 & 0 & 0 & 0 & 0 \\ 0 & 0 & 0 & 0 & 0 & 0 & 0 & 0 & 0 & 0 & 0 & 0 & 1 & 3 & 3 & 1 \\ 1 & 1 & 0 & 0 & 0 & 0 & 0 & 0 & 0 & 0 & 0 & 0 & 0 & 0 & 0 & 0 \\ 0 & 0 & 1 & 1 & 0 & 0 & 0 & 0 & 0 & 0 & 0 & 0 & 0 & 0 & 0 & 0 \\ 0 & 0 & 0 & 0 & 1 & 1 & 0 & 0 & 0 & 0 & 0 & 0 & 0 & 0 & 0 & 0 \\ 0 & 0 & 0 & 0 & 0 & 0 & 1 & 1 & 0 & 0 & 0 & 0 & 0 & 0 & 0 & 0 \\ 0 & 0 & 0 & 0 & 0 & 0 & 0 & 0 & 1 & 1 & 0 & 0 & 0 & 0 & 0 & 0 \\ 0 & 0 & 0 & 0 & 0 & 0 & 0 & 0 & 0 & 0 & 1 & 1 & 0 & 0 & 0 & 0 \\ 0 & 0 & 0 & 0 & 0 & 0 & 0 & 0 & 0 & 0 & 0 & 0 & 1 & 1 & 0 & 0 \\ 0 & 0 & 0 & 0 & 0 & 0 & 0 & 0 & 0 & 0 & 0 & 0 & 0 & 0 & 1 & 1 \end{pmatrix},$$

$$P_2H_{16}(\eta)=\frac{1}{2048}\begin{pmatrix}1&9&25&49&81&121&169&225&289&361&441&529&625&729&841&961\\1&9&25&49&81&121&169&225&287&343&391&431&463&487&503&511\\1&9&25&49&79&103&119&127&128&128&128&128&128&128&128&128\\0&0&0&0&0&0&0&0&1&9&25&49&79&103&119&127\\1&9&23&31&32&32&32&32&32&32&32&32&32&32&32&32\\0&0&0&0&1&9&23&31&32&32&32&32&32&32&32&32\\0&0&0&0&0&0&0&0&1&9&23&31&32&32&32&32\\0&0&0&0&0&0&0&0&0&0&0&0&1&9&23&31\\1&7&8&8&8&8&8&8&8&8&8&8&8&8&8&8\\0&0&1&7&8&8&8&8&8&8&8&8&8&8&8&8\\0&0&0&0&1&7&8&8&8&8&8&8&8&8&8&8\\0&0&0&0&0&0&1&7&8&8&8&8&8&8&8&8\\0&0&0&0&0&0&0&0&1&7&8&8&8&8&8&8\\0&0&0&0&0&0&0&0&0&0&1&7&8&8&8&8\\0&0&0&0&0&0&0&0&0&0&0&0&1&7&8&8\\0&0&0&0&0&0&0&0&0&0&0&0&0&0&1&7\end{pmatrix},$$

Haar wavelet integration operational matrix of general order ν is expressed as, $P_\nu=\left(P_\nu H_q(\eta)\right)H_q^{-1}(\eta)$.

Theorem 2.3.1 Consider a function $f(\eta)$ from $L^2(R)$ space. With its bounded derivative of first order, $\forall\eta\in(0,1),\left|f'(\eta)\right|\leq\lambda$. then J^{th} level error norm satisfy these inequalities.

$$\|E_J\|\leq\sqrt{\frac{\lambda}{7}}\frac{K}{2^{\sqrt{3}M}}.$$

Here λ,K are real constants and $M=2^J$ is a positive number.

Proof: Let J^{th} level error is defined as, $|E_J|=|f(\eta)-f_J(\eta)|=\sum_{l=2M+1}^{\infty}a_lh_l(\eta)$.

Where $f_J=\sum_{l=1}^{M+1}a_lh_l(\eta)$, and $\|E_J\|^2=\int_{-\infty}^{\infty}\left(\sum_{l=2M+1}^{\infty}a_lh_l(\eta),\sum_{m=2M+1}^{\infty}a_mh_m(\eta)\right)d\eta,\sum_{l=2M+1}^{\infty}\sum_{m=2M+1}^{\infty}a_la_m\int_{-\infty}^{\infty}h_l(\eta)h_m(\eta)d\eta,\|E_J\|^2\leq\sum_{l=2M+1}^{\infty}|a_l|^2$.

Since, $|a_l|\leq K2^{-3\frac{l}{2}}\max\left|f'(\eta)\right|$ and K defined as, $K=\int_0^1|\eta h_1(\eta)|\,d\eta$ for η in $\left(\frac{p}{q},\frac{p+0.5}{q}\right)$.

Thus, $\|E_J\|^2\leq\sum_{l=2M+1}^{\infty}\lambda K^2 2^{-3l}\Rightarrow\|E_J\|^2\leq\frac{1}{7}\left(\frac{\lambda K^2}{2^{3M}}\right)\Rightarrow\|E_J\|\leq\sqrt{\frac{\lambda}{7}}\frac{K}{2^{\sqrt{3}M}}$.

By above inequality, it is observed that as M increases error decreases. i.e. for Haar wavelet level of resolution is inversely proportional to error.

2.4 Haar Wavelet Integration Operational Matrix Method of Solution

The third-order nonlinear differential equation is usually expressed in its general form as,

$$f'''(\eta)=F(\eta,f,f',f''). \tag{12}$$

Approximating the highest order derivative as,

$$f'''(\eta)=\sum_{k=1}^{2M}a_kh_k(\eta)=A^TH_q(\eta), \tag{13}$$

where A^T is the Haar wavelet coefficient vector. Which is to be determined, $H_q(\eta)$ is the Haar wavelet bases matrix. Integrating **Eq. (13)** from 0 to η we get,

$$f''(\eta)=f''(0)+\sum_{k=1}^{2M}a_kP_{1,k}(\eta)=f''(0)+A^TP_1(\eta), \tag{14}$$

Integrating Eq. (14) from0 to η we get,

$$f'(\eta) = f'(0) + \eta f''(0) + \sum_{k=1}^{2M} a_k P_{2,k}(\eta) = f'(0) + \eta f''(0) + A^T P_2(\eta), \tag{15}$$

Integrating **Eq. (15)** from 0 to η gives,

$$f(\eta) = f(0) + \eta f'(0) + \frac{\eta^2}{2} f''(0) + \sum_{k=1}^{2M} a_k P_{3,k}(\eta) = f(0) + \eta f'(0) + \frac{\eta^2}{2} f''(0) + A^T P_3(\eta), \tag{16}$$

Substitute $\eta = 1aty \to \infty$ and using boundary conditions, $f''(0)$ can be determined as,

$$f''(0) = \left[f'(1) - f'(0) - \sum_{k=1}^{2M} a_k C_{1,k} \right] = \left[f'(1) - f'(0) - A^T C \right]. \tag{17}$$

Where $C = \int_0^1 P_{1,k}(\eta) d\eta$. By substituting the expressions $f(\eta), f'(\eta), f''(\eta), f'''(\eta)$ and $f''(0)$ into the provided differential **Equation (12)** and applying collocation points $\eta_r = (2r-1)/2N, r = 1, 2, ..., N$, we derive a system of nonlinear equations. Newton's Method[17] is applied to solve these N equations, resulting in the determination of the unknown Haar coefficients A^T. Substituting these unknowns in **Eq. (16)** allows us to obtain the solution to the differential equation.

2.5 Haar Wavelet Integration Operational Matrix Method of Implementation

Test Problem 2.5.1. Consider the boundary value problem (BVP) having an exact solution.

$$f''(\eta) + \left(f'(\eta)\right)^2 - 64 f(\eta) = 32, 0 < \eta < 1, f(0) = 0, f(1) = 16. \tag{18}$$

The exact solution is:

$$f(\eta) = 16\eta^2. \tag{19}$$

We solve **Eq. (18**) using the HWIOMM as outlined in section 2.4. We obtain a nonlinear system of algebraic equations as follows,

$$A^T H(\eta) + \left[(16 - A^T P_2(1)) + A^T P_1(\eta) \right]^2 - 64 \left[(16 - A^T P_2(1)) \eta + A^T P_2(\eta) \right] = 32. \tag{20}$$

By solving these systems of N algebraic equations using Newton's method[17], we can determine the unknown coefficients. Substituting these coefficients into the equations gives a solution for the above BVP.

To demonstrate the effectiveness of the proposed approach, we present the nonlinear boundary value problem (BVP) described in **Eq. (18**), with its exact solution given in **Eq. (19**). The results obtained using HWIOMM closely match the exact solution with remarkable precision, comparable to the Range-Kutta Fehlberg 4^{th} -5^{th} Method (RKF45). These findings are detailed in Table 1 and Figure 1, with error estimation provided in Table 2.

Table 2 clearly illustrates the error analysis for different levels of resolution. We can see that error diminishes with increasing resolution.

Turbulent Boundary Layer Fluid Flow Problem 2.5.2. The diagram depicts the formation of the boundary layer in regions of turbulent flow, as well as the transition from laminar to turbulent layers, as shown in Figure 2. At high Reynolds numbers, turbulent flow persists boundary layer characteristics. The occurrence of turbulent flows relies on reduced viscosity or higher fluid velocity. In these situations, there is significant chaotic motion near the surface. Due to the complexities of fluctuation in velocity and pressure, it is necessary to consider the time average motion of the turbulent flow.

The Navier-Stokes equation for turbulent flow, i.e. Reynolds averaging equation of motion and continuity equation of two-dimensional, time-independent incompressible fluid of turbulent boundary layer is given by following boundary value problems.

$$\frac{\partial \overline{u}}{\partial x} + \frac{\partial \overline{v}}{\partial y} = 0, \tag{21}$$

$$\overline{u}\frac{\partial \overline{u}}{\partial x} + \overline{v}\frac{\partial \overline{u}}{\partial y} = \frac{-1}{\rho}\frac{\partial P}{\partial y} + \mu \frac{\partial^2 \overline{u}}{\partial y^2} - \frac{\partial}{\partial y} < u'v' > . \tag{22}$$

Table 1. Comparison of HWIOMM solution to the exact solution and RKF45 solution for $N = 16$ of test problem 2.5.1

η	**Exact solution**	**HWIOMM Solution**	**HWIOMM Absolute error**	**RKF45 Solution**	**RKF45 Absolute error of**
0.031250	0.01562500000	0.01562500005	5.646E-11	0.014865804	7.591E-4
0.093750	0.1406250000	0.1406250001	1.694E-10	0.138346271	2.227E-3
0.156250	0.3906250000	0.3906250002	2.823E-10	0.386825515	3.799E-3
0.218750	0.7656250000	0.7656250003	3.952E-10	0.760303990	5.321E-3
0.281250	1.265625000	1.2656250005	5.082E-10	1.258782071	6.842E-3
0.343750	1.890625000	1.8906250006	6.211E-10	1.882259977	8.365E-3
0.406250	2.640625000	2.6406250007	7.340E-10	2.630737800	9.887E-3
0.468750	3.515625000	3.5156249992	7.792E-10	3.504215572	1.140E-2
0.531250	4.515625000	4.5156249991	8.502E-10	4.502693302	1.293E-2
0.593750	5.640625000	5.6406249990	9.499E-10	5.626170994	1.445E-2
0.656250	6.890625000	6.8906249989	1.050E-9	6.874648656	1.597E-2
0.718750	8.265625000	8.2656249988	1.150E-9	8.248126297	1.749E-2
0.781250	9.765625000	9.7656249987	1.249E-9	9.746603934	1.902E-2
0.843750	11.39062500	11.390624998	1.349E-9	11.37008159	2.054E-2
0.906250	13.14062500	13.140624998	1.450E-9	13.11855928	2.206E-2
0.968750	15.01562500	15.015624998	1.550E-9	14.99203705	2.358E-2

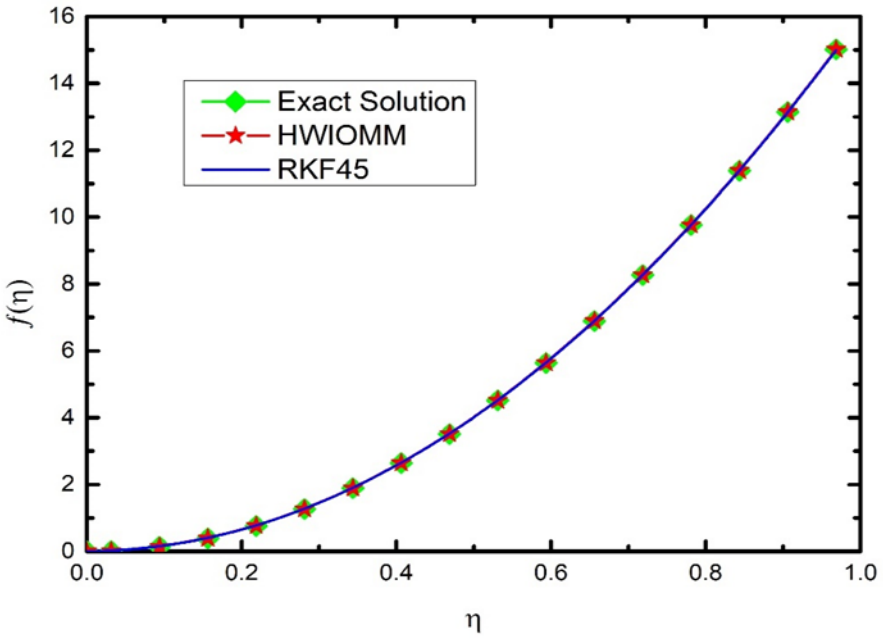

Fig 1. Results of HWIOMM and RKF45 with the exact solution of test problem 2.5.1

Table 2. Error analysis L_∞ of HWIOMM solution for the test problem 2.5.1

J	N	L_∞
2	08	1.75482E-8
3	16	1.54999E-9
4	32	3.93754E-10
5	64	3.98396E-10
6	128	4.14358E-10
7	256	4.70911E-10

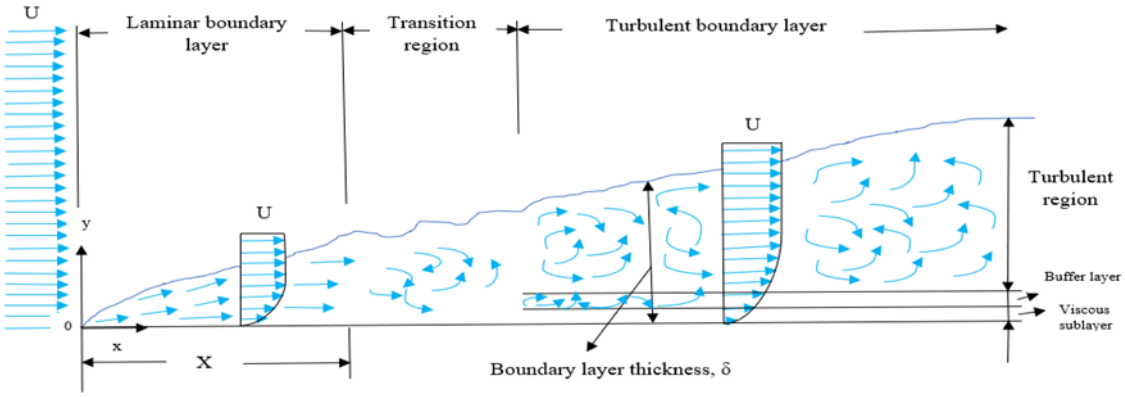

Fig 2. Formation of turbulent boundary layer

Here, $\overline{u}$ and $\overline{v}$ are the velocity components, representing the mean stream-wise and mean wall-normal velocities respectively, along x axis and normal direction parallel to y axis. μ indicates kinematic viscosity, which depends on the temperature of the fluid, $\frac{dP}{dx}$ is the pressure gradient, ρ is the density, and $< u'v' >$ is an additional stress known as the apparent stress of the fluid. In turbulent flow, total stress is made up of regular viscous stress and apparent stress or Reynolds stress. Initially, fluid near the wall will be at rest, which means velocities $\overline{u}$ and $\overline{v}$ are zero. As the fluid resides from the wall as $y \to \infty$ velocity $\overline{u}$ is equal to free stream velocity U. Thus, boundary conditions for the boundary layer equation will be, $\overline{u} = \overline{v} = 0$ when $y = 0$ and $\overline{u} \to U$ when $y \to \infty$. At constant pressure, and using the Boussinesq approximation for turbulent shear stress, **Eq. (22)** reduces to,

$$\overline{u}\frac{\partial \overline{u}}{\partial x} + \overline{v}\frac{\partial \overline{u}}{\partial y} = \frac{1}{\rho}(\mu + \mu_t)\frac{\partial^2 \overline{u}}{\partial y^2}. \tag{23}$$

Where μ_t is eddy viscosity, which is a function of flow and μ is a function of temperature.

We transform **Eq. (23)** to a suitable form, by considering the stream function ψ we have,

$$\overline{u} = \frac{\partial \psi}{\partial y}, \overline{v} = \frac{-\partial \psi}{\partial x}. \tag{24}$$

Introducing similarity variable η and stream function ψ as,

$$\eta = \frac{y}{\delta} = \frac{y}{\left(\frac{\mu_t}{\rho U}\right)^{\frac{1}{n}} x^{\frac{n-1}{n}}}, \text{ and } \psi = -\int \overline{u} dy = -c\left(\frac{\mu_t}{\rho}\right)^{\frac{1}{n}} (Ux)^{\frac{(n-1)}{n}} f(\eta). \tag{25}$$

Using **Eq. (24)** and **(25)** simplified equation is,

$$f'''(\eta) + \left[\alpha \Re^{\frac{n-2}{n}}\right] f(\eta) f''(\eta) = 0. \tag{26}$$

Defining Reynolds number $\Re$ as $\Re \frac{\rho U\, x}{\mu_t}$ and $\alpha = c^{2\,\frac{(n-1)}{n}}$. Since $c \neq 0$ for all $n > 2$ this implies $\alpha > 0$. Boundary conditions are $f(0) = f'(0) = 0, f'(\infty) = 1$.

Consider the generic turbulent boundary layer fluid flow equation given in **Eq. (26)**, along with its boundary conditions. As discussed in section 2.4, a similar procedure is followed for solving the considered fluid problem of the turbulent boundary layer. We obtain a nonlinear system of algebraic equations. By using collocation points $\eta_r = (2r-1)/2N, r = 1, 2, ..., N$, and substituting values of $f(\eta)$, $f''(\eta)$ and $f''(0)$ in **Eq. (26)**, we obtain the following equation.

$$A^T H(x) + \alpha \Re^{\frac{n-2}{n}} \left[\frac{x^2}{2} + A^T P_3(x) - \frac{x^2}{2} A^T P_2(1) \right] + 1 + A^T P_1(x) - A^T P_2(1) = 0. \tag{27}$$

Newton's method [17] is applied to solve N nonlinear algebraic equations of **Eq. (27)** and unknown Haar wavelet coefficients are obtained. Substituting these unknowns, the numerical solution of equations $f(\eta), f'(\eta), f''(\eta)$ can be determined.

3 Results and Discussion

In this present analysis, the HWIOMM is developed for the numerical solution of nonlinear differential equations of turbulent boundary layer. Initially, a test problem with exact solution is solved to validate the proposed method. The results obtained by HWIOMM are highly accurate and convergent, even with a small number of grid points. It has been observed that the HWIOMM solution is very close to the exact solution, demonstrating significantly better accuracy compared to the RKF45 method. From **Table 1, 2** and Figure 1, it is clear that the HWIOMM solution shows strong agreement with the exact solution. Further, HWIOMM is utilised for solving turbulent boundary layer fluid flow problem. The equation derived in **Eq. (26)**, along with the boundary condition, represents an enhanced Blasius equation for turbulent flow. For $n = 2$ equation simplifies to the general equation for Streamline flow given by Cortell [18]. We obtained the solution of the equation for $\alpha = \frac{1}{2}$ by HWIOMM and our results are observed to be very close to those obtained by Howarth [19].

To validate HWIOMM and the generalized Blasius equation. The solution given by Howarth [19] and the numerical solution obtained are presented in Table 3 and Figure 3.

Table 3. Comparison of f, f', f'' values by HWIOMM for $n = 2 \wedge \alpha = \frac{1}{2}$ with Howarth's [19] results

η	HWIOMM			Howarth's [19] result		
	$f(\eta)$	$f'(\eta)$	$f''(\eta)$	$f(\eta)$	$f'(\eta)$	$f''(\eta)$
0	0	0	1.3282	0	0	1.3282
0.1	0.0066	0.1328	1.3281	0.0066	0.1328	1.3280
0.2	0.0265	0.2656	1.3245	0.0265	0.2655	1.3259
0.3	0.0597	0.3984	1.3183	0.0597	0.3979	1.3203
0.4	0.1061	0.5312	1.3077	0.1061	0.5294	1.3095
0.5	0.1656	0.6641	1.2914	0.1655	0.6598	1.2920
0.6	0.2381	0.7969	1.2685	0.2379	0.7876	1.2664
0.7	0.3230	0.9297	1.2383	0.3229	0.9125	1.2315
0.8	0.4209	1.0325	1.1878	0.4203	1.0335	1.1867
0.9	0.5316	1.1445	1.1330	0.5295	1.1495	1.1317
1	0.6536	1.2682	1.0684	0.6500	1.2595	1.0670

Fluid model describes the turbulent boundary layer flow at high Reynolds numbers, where Reynolds number plays a trivial role in determining flow characteristics. Usually flows with high Reynolds number is considered to be turbulent. Based on Reynolds number flow regimes can be analysed. If the Reynolds number is less than 2000, the flow is considered to be laminar, for a Reynolds number more than 4000, the flow is turbulent. And Reynolds number that falls between 2000 and 4000 is categorized as transitional flow. Thus, flows with a Reynolds number greater than 4000 are considered to be turbulent flows. For specificαacceleration is analysed for higher Reynolds numbers and is shown in **Table 4**.

From Figure 4, it can be observed that for $\alpha = 0.14112 \wedge n = 5$, acceleration increases with an increase in Reynolds number. Similarly, for$\alpha = 0.0128 \wedge n = 9$. It is observed that due to the greater momentum of fluid particles, there is a rise in inertial force and a reduction in viscosity. As a result, acceleration increases with the increase in Reynolds number and acceleration less increases with the rise of the integer number$n$. To analyse the velocity profile of the governing equation, HWIOMM is

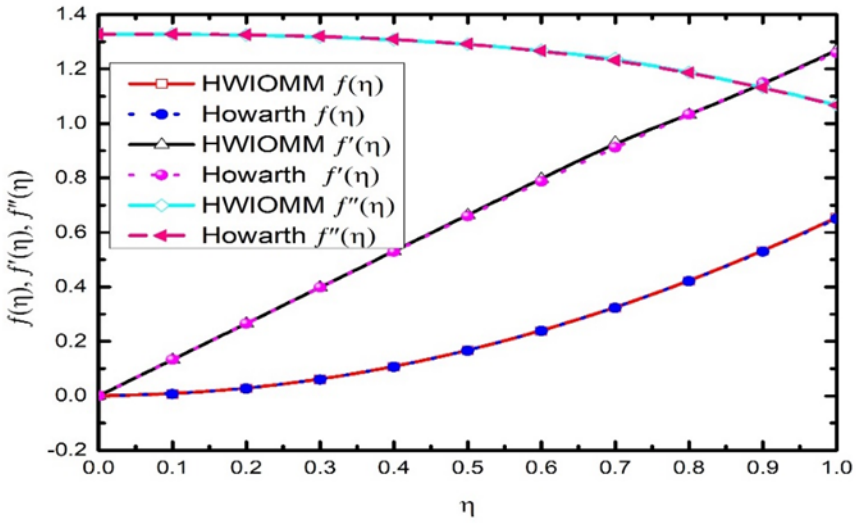

Fig 3. Result of f, f', f'' by HWIOMM for $n = 2 \wedge \alpha = \frac{1}{2}$

Table 4. Comparison values of $f''(0)$ for $\alpha = 0.14112 \wedge n = 5$ and $\alpha = 0.0128 \wedge n = 9$

Reynolds no. Re	**Value of** αRe	$f''(0)$ for $\alpha = 0.14112 \wedge n = 5$	$f''(0)$ for $\alpha = 0.0128 \wedge n = 9$
5000	23.3868	2.2735	1.5090
10000	35.4477	2.6001	1.9154
20000	53.7287	3.0636	2.5031
30000	68.5269	3.4501	2.9319
40000	81.4375	3.79	3.2803
50000	93.1044	4.098	3.5791
60000	103.8674	4.3645	3.8435
70000	113.9324	4.527	4.0757
80000	123.4362	4.6411	4.2101

implemented. The comparison of velocity with high Reynolds numbers for various values of n is given. It is observed that there is an increase in velocity with an increase in Reynolds number and less increase in velocity with an increase in n shown in Figure 5. The study emphasises the relation between the Reynolds number and the changing behaviour of fluid systems from laminar to turbulent flow. In laminar flow, acceleration typically rises as the Reynolds number does. However, in turbulent flow, drag resistance and energy loss cause the acceleration to gradually decrease as the Reynolds number rises after increasing to a certain point, observed in Figure 6.

4 Conclusion

In this article, the Haar wavelet integration operational matrix method (HWIOMM) is developed to solve turbulent boundary layer equations under the consideration of a constant pressure gradient. Initially, we present nonlinear BVP having an exact solution to justify the proposed method. The HWIOMM is validated by contrasting the outcomes with RKF45, and our results show that the HWIOMM solutions are more accurate and closely aligned with the exact solutions. Furthermore, we analyze the error rates at different levels of resolution, and it is observed that HWIOMM exhibits a lower error rate, even with smaller grid points. The considered turbulent flow problem is solved using HWIOMM for $n = 2 \wedge \alpha = \frac{1}{2}$. The acquired solutions are contrasted with the existing numerical findings, and the results are found to be more accurate and coincide with existing literature. The study of acceleration for higher Reynolds numbers for specific values of αhas been examined and noted that the acceleration increases with an increase in Reynolds number. Further, is found to increase with the increase in Reynolds

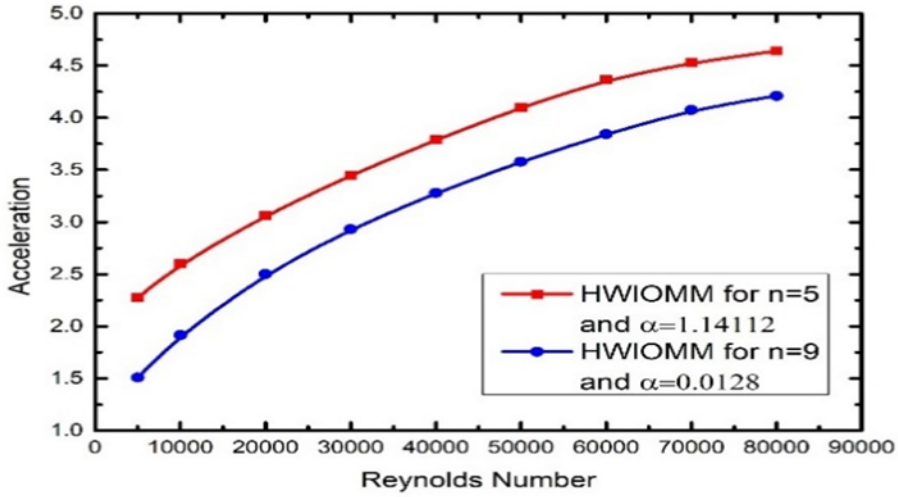

Fig 4. Variation of acceleration for increasing values of Reynolds Numbers

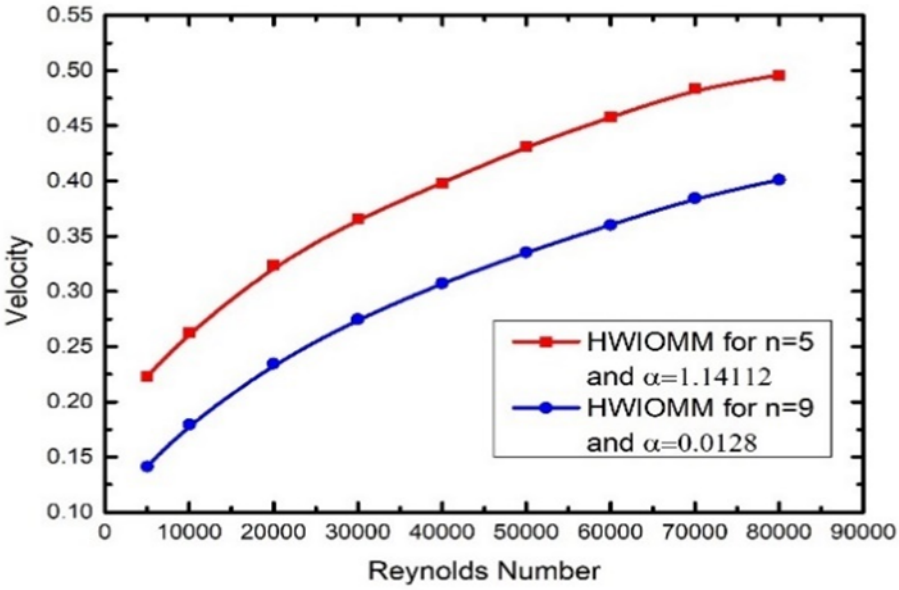

Fig 5. Variation of velocity for increasing values of Reynolds Numbers

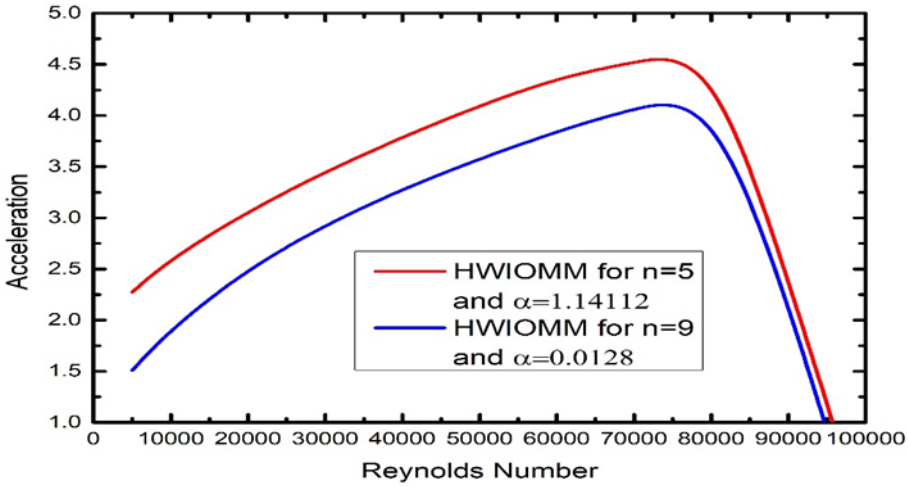

Fig 6. Variation of acceleraton for increasing values of Reynolds Numbers

number and after reaching a certain limit acceleration gradually drops with increasing Reynolds number. The presented results imply that the method provides an efficient, reliable and simple method for solving such complex problems.

5 Acknowledgement

The authors thank Government of India Ministry of Science and Technology-Innovation in Science Pursuit for Inspired Research (DST-INSPIRE), New Delhi. No. DST/INSPIRE Fellowship/2022/IF220213, Dated: 18-10-2023, for the financial support of this work.

6 Conflicts of Interest

The authors declare that there is no conflict of interest.

References

1) Schlichting H, Gersten K. *Boundary Layer Theory*. New York. Springer. 2017. doi:https://link.springer.com/book/10.1007/978-3-662-52919-5.
2) Blasius H. Grenzschichten in flü sigkeiten MIT kleiner reibung. *Journal of Applied Mathematics and Physics*. 1908;56:1–37.
3) Khanfer A, Bougoffa L, Bougouffa S. Analytic Approximate Solution of the Extended Blasius Equation with Temperature-Dependent Viscosity. *Journal of Nonlinear Mathematical Physics*. 2023;30:287–302. doi:https://doi.org/10.1007/s44198-022-00084-3.
4) Huang J, Duan L, Coudari MM. Direct numerical simulation of hypersonic turbulent boundary layers: effect of spatial evolution and Reynolds number. *Journal of Fluid Mechanics*. 2022;937:1–49. A30. doi:https://doi.org/10.1017/jfm.2022.80.
5) Laguarda L, Hickel S, Schrijer FJ, Oudheusden BW. Reynolds number effects in shock-wave/turbulent boundary-layer interactions. *Journal of Fluid Mechanics*. 2024;989:1–49. A20. doi:https://doi.org/10.1017/jfm.2024.361.
6) Camillo GP, Wagner A, Toki T, Scalo C. Combined Experimental and Numerical Investigation of a Hypersonic Turbulent Boundary Layer by Means of FLDI and Large-Eddy Simulations. *Aerospace*. 2023;10:570–601. doi:https://doi.org/10.3390/aerospace10060570.
7) Gao M, Appel D, Beck A, Munz CD. A high-order fluid–structure interaction framework with application to shock-wave/turbulent boundary-layer interaction over an elastic panel. *Journal of Fluids and Structures*. 2023;121:103950. doi:https://doi.org/10.1016/j.jfluidstructs.2023.103950.
8) Huang R, Liu W, Cheng J, Wu J. Measurement of hypersonic turbulent boundary layer on a flat plate using cylindrical focused laser differential interferometer. *Physics of Fluids*. 2023;35:035121. doi:https://doi.org/10.1063/5.0141681.
9) Salvadore F, Memmolo A, Modesti D, Posta GD, Bernardini M. Direct numerical simulation of a microramp in a high-Reynolds number supersonic turbulent boundary layer. *Physical Review Fluids*. 2023;8:110508. doi:https://doi.org/10.1103/PhysRevFluids.8.110508.
10) Knopp T, Eça L, Toxopeus SL, Fritsch D, Gargiulo A, Lowe KT, et al. Errors and uncertainties in CFD validation for nonequilibrium turbulent boundary layer flows at high Reynolds numbers. *Journal of Turbulence*. 2024;25:399–422. doi:https://doi.org/10.1080/14685248.2024.2360195.
11) Sunthrayuth P, Aljahdaly NH, Ali A, Shah R, Mahariq I, Tchalla AM. Φ-Haar Wavelet Operational Matrix Method for Fractional Relaxation-Oscillation Equations Containing Φ-Caputo Fractional Derivative. *Journal of Function Spaces*. 2021;p. 7117064. doi:https://doi.org/10.1155/2021/7117064.

12) Verma AK, Kumar N, Tiwari D. Haar wavelets collocation method for a system of nonlinear singular differential equations. *Engineering Computations*. 2021;38(2):659–698. doi:https://doi.org/10.1108/EC-04-2020-0181.
13) Mohammad NA, Sabawi YA, Hasso M. Numerical solution based on the Haar wavelet collocation method for partial integro-differential equations of Volterra type. *Arab Journal of Basic and Applied Sciences*. 2024;31(1):614–628. doi:https://doi.org/10.1080/25765299.2024.2419145.
14) Preetham MP, Kumbinarasaiah S. A numerical study of two-phase nanofluid MHD boundary layer flow with heat absorption or generation and chemical reaction over an exponentially stretching sheet by Haar wavelet method. *Numerical Heat Transfer, Part B: Fundamentals*. 2023;85(6):706–735. doi:https://doi.org/10.1080/10407790.2023.2253364.
15) Shiralashetti SC, Badiger P. Haar wavelet algebraic multigrid method for the numerical solution of squeeze film lubrication problem of porous journal bearings with couple stress fluid. *Palestine Journal of Mathematics*. 2023;12(2):578–596. Available from: https://pjm.ppu.edu/sites/default/files/papers/PJM_12(2)_2023_578_to_596.pdf.
16) Shiralashetti SC, Lamani L. Numerical solution of stochastic ordinary differential equations using Haar wavelet collocation method. *Journal of Interdisciplinary Mathematics*. 2022;25(2):195–211. doi:https://doi.org/10.1080/09720502.2021.1874085.
17) Burden RL, Flaires JD. Numerical Analysis. 9th ed. Boston, MA. Cengage Learning, Brooks/Cole. 2011.
18) Cortell R. Numerical solutions of the classical Blasius flat-plate problem. *Applied Mathematics and Computation*. 2005;170(1):706–710. doi:https://doi.org/10.1016/j.amc.2004.12.037.
19) Howarth L. On the solution of laminar boundary layer equations. *Proceedings of the Royal Society of London Series A, Mathematical and Physical Sciences*. 1938;164:547–579. doi:https://doi.org/10.1098/rspa.1938.0037.